

Article

Texture segmentation: an objective comparison between traditional and deep-learning methodologies

Cefa Karabağ¹, Jo Verhoeven^{2,3}, Naomi Rachel Miller² and Constantino Carlos Reyes-Aldasoro^{1,*}

¹ Department of Electrical and Electronic Engineering, Research Centre for Biomedical Engineering, School of Mathematics, Computer Science and Engineering, City, University of London, London EC1V 0HB, UK

² School of Health Sciences, Division of Language & Communication Science, Phonetics Laboratory, City, University of London, UK; johan.verhoeven.1@city.ac.uk, naomi-rachel.miller@city.ac.uk

³ Department of Linguistics CLIPS, University of Antwerp, Antwerp, Belgium; jo.verhoeven@uantwerpen.be

* Correspondence: reyes@city.ac.uk (CCRA)

Abstract: This paper compares a series of traditional and deep learning methodologies for the segmentation of textures. Six well-known texture composites first published by Randen and Husøy were used to compare traditional segmentation techniques (co-occurrence, filtering, local binary patterns, watershed, multiresolution sub-band filtering) against a deep-learning approach based on the U-Net architecture. For the latter, the effects of depth of the network, number of epochs and different optimisation algorithms were investigated. Overall, the best results were provided by the deep-learning approach. However, the best results were distributed within the parameters, and many configurations provided results well below the traditional techniques.

Keywords: Texture; Segmentation; Deep Learning

1. Introduction

Texture, and more specifically textural characteristics in images, has been widely studied in the past decades as texture is one of the most important features present in images and can be used for feature extraction [1–8] and classification and segmentation [9–14]. The areas of study where texture is present range from crystallographic texture [15], stratigraphy [16,17], food science of potatoes [18] or apples [19], patterned fabrics [20] to natural stone industry [21]. In medical imaging, there is a large volume of research which exploits the use of texture for different purposes like segmentation of classification in most acquisition modalities like magnetic resonance imaging (MRI) [22–26], ultrasound [27,28], computed tomography (CT) [29–31], microscopy [32,33] and histology [34]. There are numerous approaches to texture: Haralick's co-occurrence matrix [4,5] on the spatial domain, Gabor filters [35–37] and ordered pyramids [8] on the spectral domain, wavelets [38,39] or Markov random fields [3,40].

In recent years, advances in artificial intelligence have been revolutionised image processing tasks. Several deep learning approaches [41–43] have achieved outstanding results in difficult tasks such as those of the ImageNet Large Scale Visual Recognition Challenge (ILSVRC) [44]. Convolutional Neural Networks (CNNs) are well suited to analyse textures as their repetitive patterns can be learned and identified by filter banks [45]. The U-Net architecture proposed by Ronneberger [46] has become a very widely used tool for segmentation and analysis reaching thousands of citations in few years since it was published. U-Nets have been used widely, for instance, road extraction [47], singing voice separation [48], automatic brain tumour detection and segmentation [49] and cell counting, detection, and morphometry [50]. The success of these deep learning approaches in very different areas invite for its application on texture analysis.

In this work, a U-Net architecture for the segmentation of textures is implemented and objectively compared against several popular traditional segmentation strategies. To perform an objective

33 comparison, six well-known texture composites from the Brodatz [51] album, first published by Randen
34 and Husøy [52], are segmented with U-Nets of different configurations and parameters and the results
35 compared against previously published results. The effects of the configuration of the networks, namely,
36 number of epochs, depth of the network in the number of layers, and type of optimisation algorithm
37 are assessed. All the programming was performed in Matlab® (The Mathworks™, Natick, USA) and
38 the code is freely available through GitHub (<https://github.com/reyesaldasoro/Texture-Segmentation>).

39 2. Materials and Methods

40 2.1. Texture composite images

41 Six composite texture images were segmented in this work (Fig. 1). The first five composites are
42 images of 256×256 pixels and consist of five different textures whilst the last one is 512×512 pixels
43 and is formed with 16 different textures. The masks with which these were formed are shown in Fig. 2.
44 It should be highlighted that these textures have been histogram equalised prior to the arrangement
45 and thus they cannot be distinguished by the general intensity of each region. Furthermore, whilst
46 some textures are easy to distinguish, there are some that are quite challenging, for instance, the
47 difference between the central and bottom regions in Fig. 1(c) or the top left corners of Fig. 1(d,e).

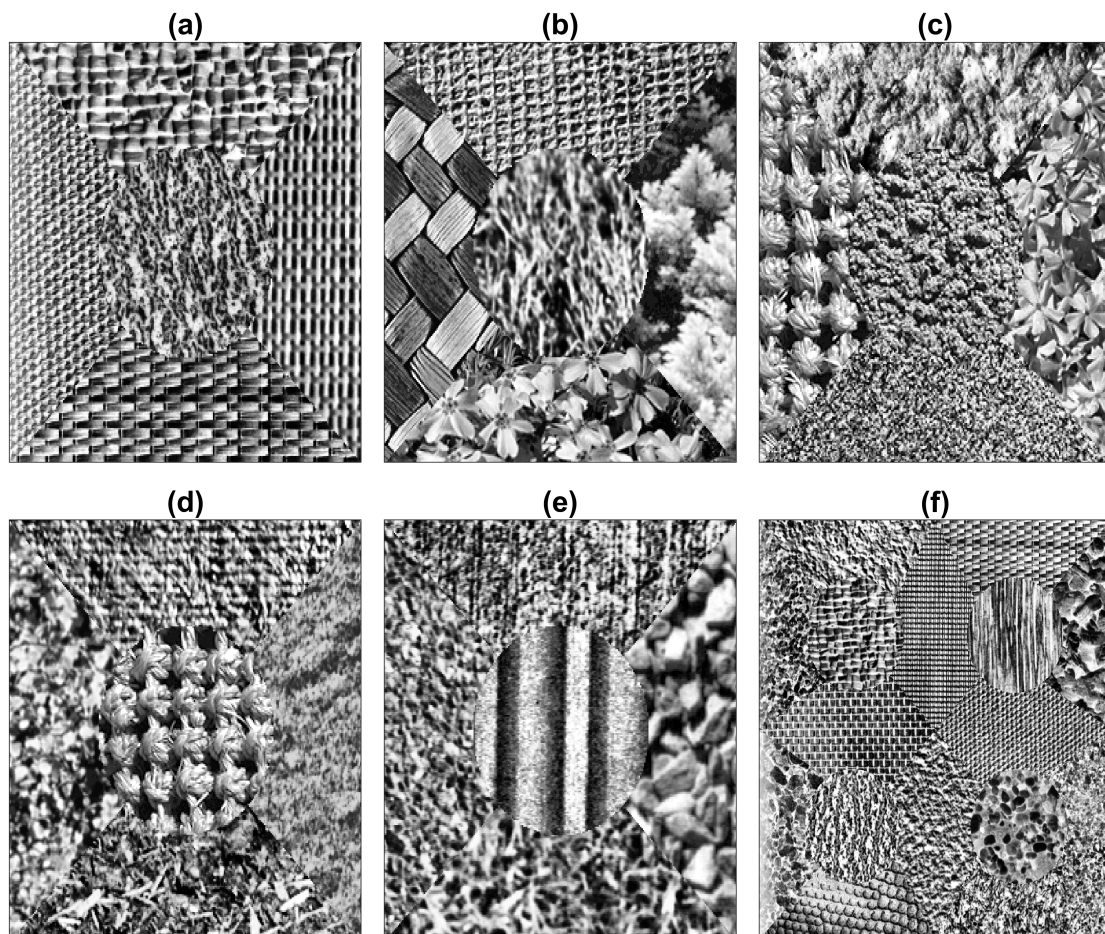


Figure 1. Six composite texture images. (a–e) Texture arrangements with five textures. (f) Texture arrangement with sixteen textures. Notice first, that individual textures have been histogram equalised and thus each region cannot be distinguished by the intensity, and second, some textures are easier to distinguish (e.g. (a)) than others (e.g. (d)).

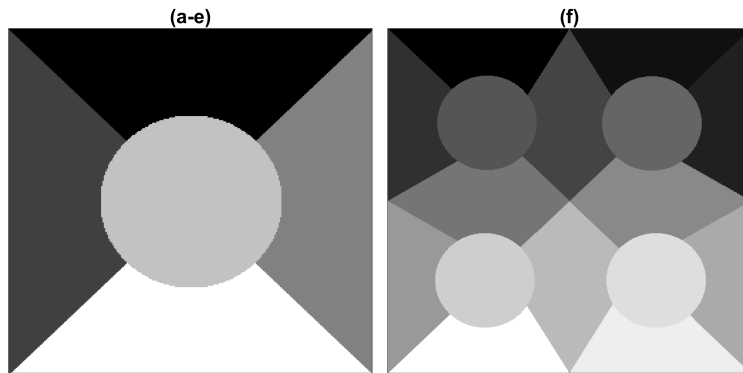


Figure 2. (a) Mask corresponding to texture arrangements of Figs. 1(a-e). (b) Mask corresponding to texture arrangements of Fig. 1(f).

48 *2.2. Training data*

49 The training data in [52] is provided separately and is shown in Fig. 3 for the first five composites
50 and in Fig. 4 for the last case. For the purpose of training the U-Nets, the training images were
51 tessellated into sub-regions of 32×32 pixels each.

52 Pairs of textures and labels were constructed simultaneously in the following way: two training
53 images were selected. Sub-regions of each image were selected and for every pair of the sub-regions,
54 half of each was selected and placed together so that a new 32×32 patch with both textures was
55 created with a corresponding 32×32 patch with the classes. The patches were created with diagonal,
56 vertical and horizontal pairs. The training images were traversed horizontally and vertically without
57 overlap creating numerous training pairs. A montage of the texture pairs and labels corresponding to
58 Fig. 1(a) is illustrated in Fig. 5. All pairs between classes were considered i.e. 1 – 2, 1 – 3, 1 – 4, 1 –
59 5, 2 – 1, 2 – 3, . . . , 5 – 3, 5 – 4. In total, 2,940 patches were created for the five composites with five
60 textures and 35,280 were created for the composite with sixteen textures.

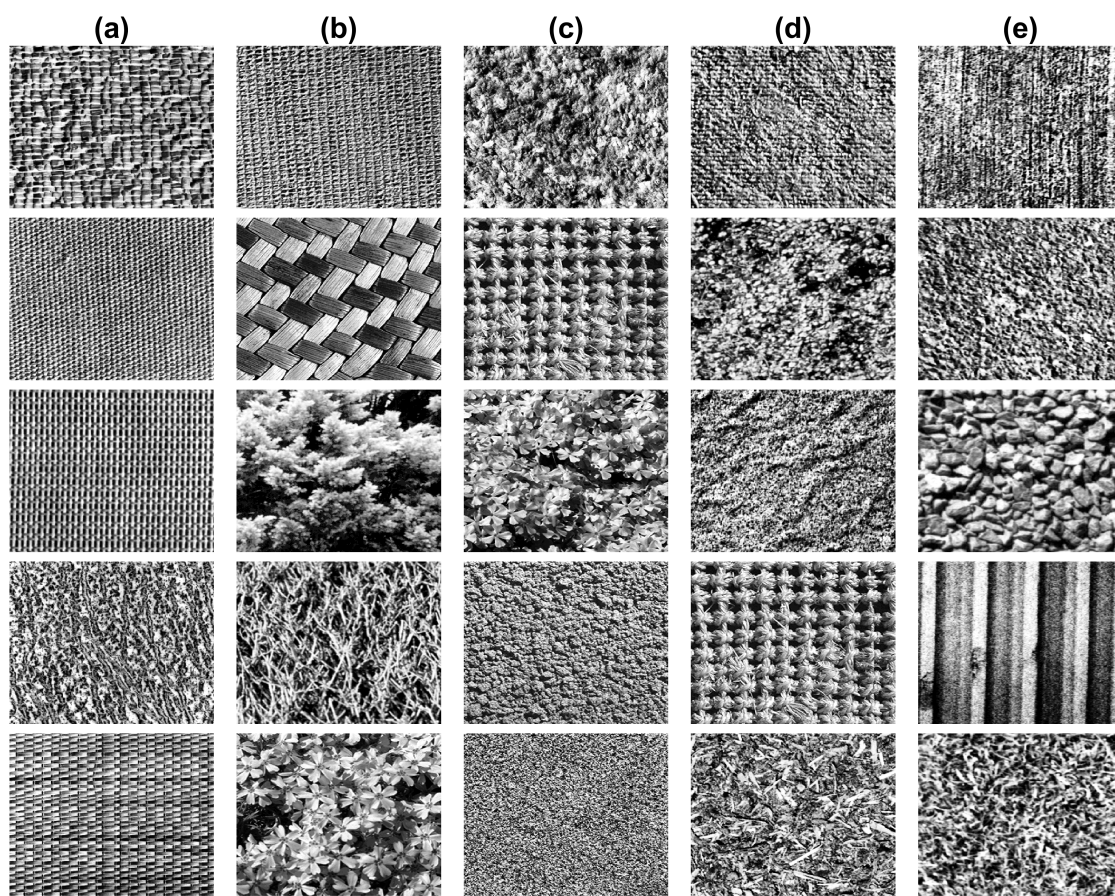


Figure 3. Training images corresponding to the texture arrangements of Figs. 1(a-e).

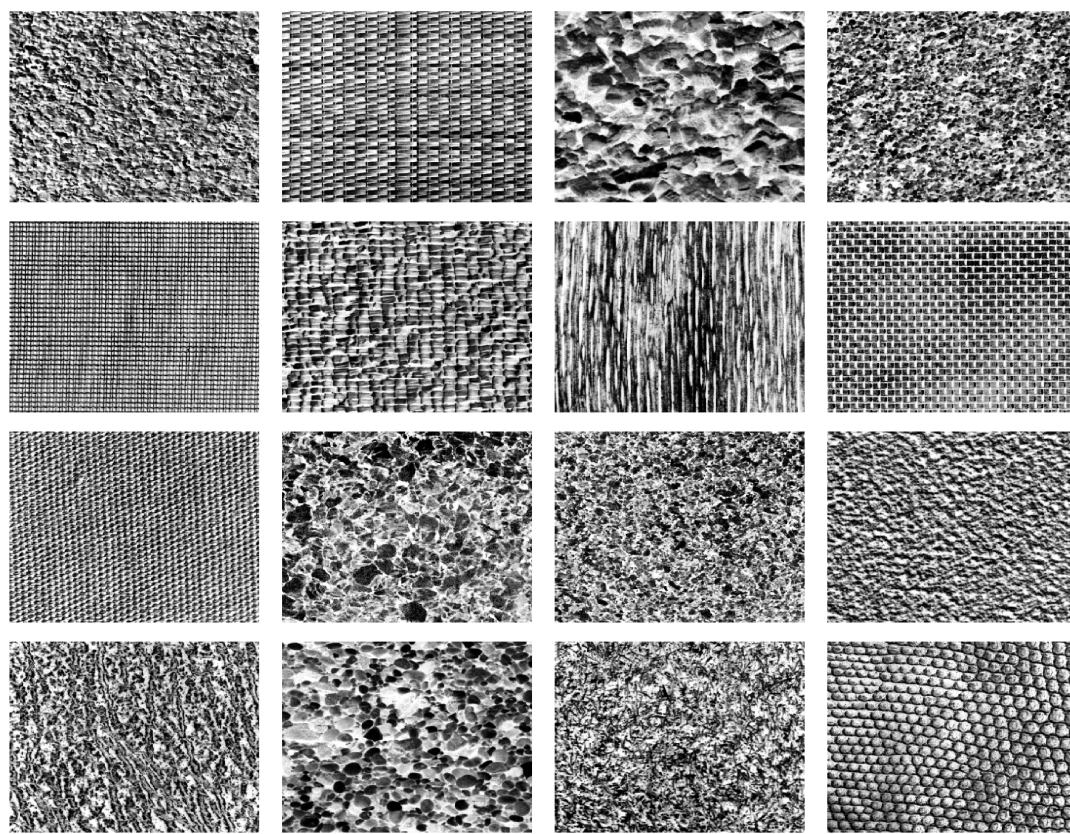


Figure 4. Training images corresponding to the texture arrangements of Fig. 1(f).

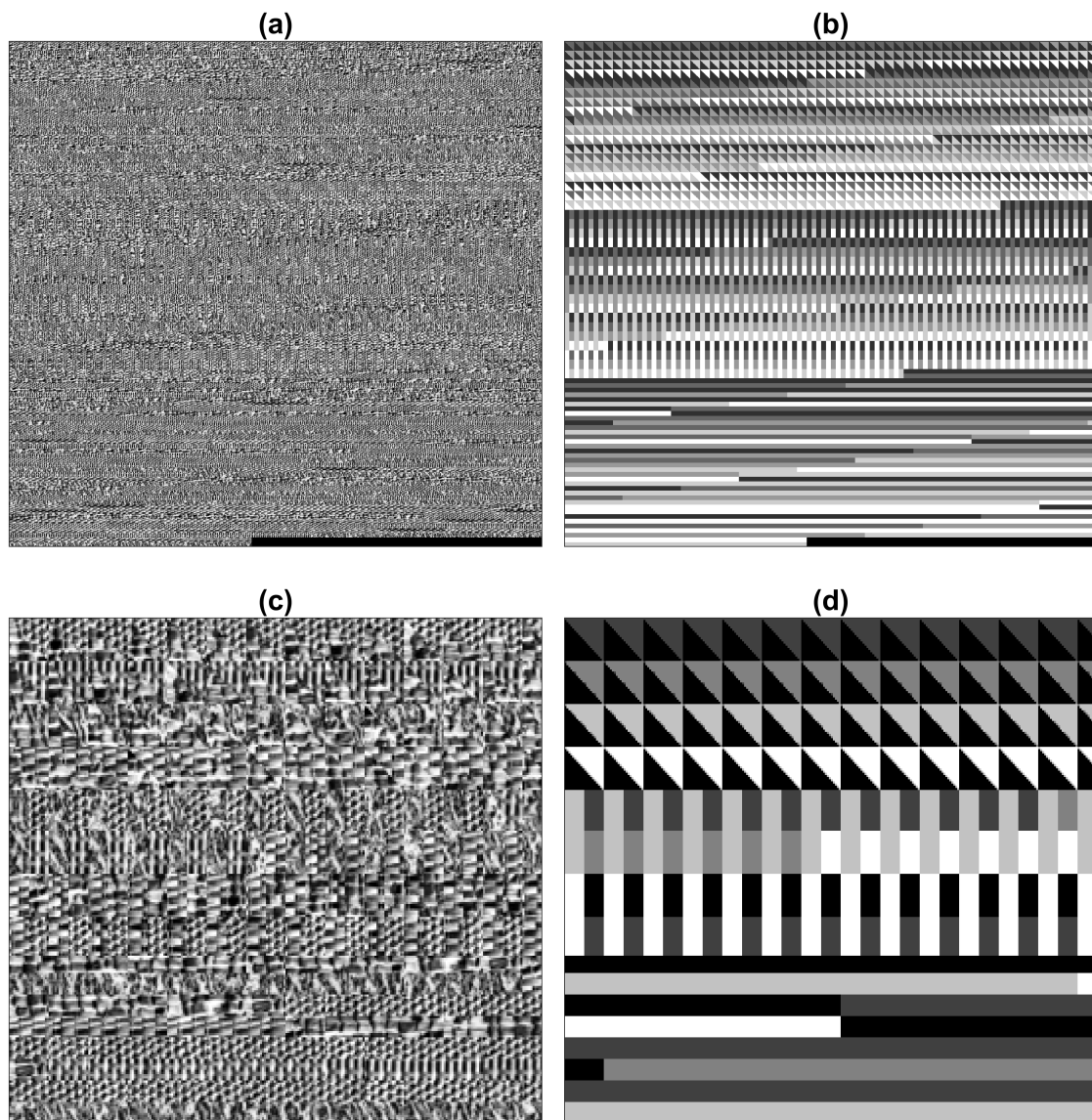


Figure 5. Montages of the texture pairs created to train the deep learning networks. Training images shown in Figs. 3,4 were tessellated and arranged in diagonal, vertical and horizontal pairs. (a) Texture pairs. (b) Labels. (c) Detail of the texture pairs. (d) Detail of the labels.

61 2.3. Texture segmentation algorithms

62 For this paper, we compared the results of the following texture segmentation algorithms:
 63 co-occurrence matrices [5], filtering [52], Local Binary Patterns (LBP) [53], watershed [54] and
 64 multiresolution sub-band filtering (MSBF) [8] against a U-Net architecture [46]. As the traditional
 65 algorithms have been thoroughly described in the literature, this section will only describe the
 66 configuration of the U-Net. For a review of traditional texture techniques, the reader is referred
 67 to any of the following reviews [55–57].

68 The basic U-Net architecture was formed with the following layers: *Input*, *Convolutional*, *ReLU*,
 69 *Max Pooling*, *Transposed Convolutional*, *Convolutional*, *Softmax* and *Pixel Classification*. Two levels of
 70 depth were investigated by repeating the downsampling and upsampling blocks in the following
 71 configurations:

72 15 layers:

73 Input,

74 Convolutional, ReLu, Max Pooling,
75 Convolutional, ReLu, Max Pooling,
76 Convolutional, ReLu,
77 Transposed Convolutional, Convolutional,
78 Transposed Convolutional, Convolutional,
79 Softmax,
80 Pixel Classification
81

82 20 layers:

83 Input,
84 Convolutional, ReLu, Max Pooling,
85 Convolutional, ReLu, Max Pooling,
86 Convolutional, ReLu, Max Pooling,
87 Convolutional, ReLu,
88 Transposed Convolutional, Convolutional,
89 Transposed Convolutional, Convolutional,
90 Transposed Convolutional, Convolutional,
91 Softmax,
92 Pixel Classification.

93
94 The image input layer was configured for the 32×32 patches. The convolutional layers consisted
95 of 64 filters of size 3 and padding of 1. The pooling size was 2 with stride of 2. The transposed
96 convolutional had a filter size of 4, stride of 2 and cropping of 1. The number of epochs evaluated
97 were 10, 20, 50, 100. The following optimisation algorithms were analysed: stochastic gradient descent
98 (sgdm), Adam (Adam) [58] and Root Mean Square Propagation (RMSprop). One last investigation
99 was performed by training the 20 layer network two separate times to investigate the variability of the
100 process.

101 3. Results

102 For each image, the networks were trained with the 3 different optimisation algorithms, 3 layer
103 configurations and 4 epoch numbers, for a total of 36 different combinations. Thus for the 6 composites
104 images there were 216 results. The misclassification of each segmentation was measured against the
105 ground truth as the percentage of pixels classified incorrectly. These results are summarised in table 1.

106 The best results for each image were selected and compared against traditional methodologies
107 and are shown in table 2. The results are illustrated graphically in two ways. Fig. 6 shows segmented
108 the classes overlaid as different colours over the original textured images. Fig. 7 shows correctly
109 segmented pixels in white and the misclassified pixels in black.

Table 1. Comparative misclassification (%) results of the different U-Net configurations. (Bold and underline denotes the best result for each image).

Method			Figures					
Layers	Optimisation Algorithm	Epochs	a	b	c	d	e	f
15	sgdm	10	6.8	21.5	40.8	31.2	27.2	20.9
20	sgdm	10	33.0	59.0	74.3	79.1	77.3	41.9
20	sgdm	10	71.9	62.9	74.3	78.8	72.1	39.0
15	Adam	10	3.2	10.4	7.9	<u>7.1</u>	17.8	19.3
20	Adam	10	7.4	15.5	46.5	25.0	45.1	94.2
20	Adam	10	6.4	15.5	36.0	21.1	26.7	32.9
15	RMSprop	10	5.1	<u>8.9</u>	14.0	18.3	12.1	17.6
20	RMSprop	10	5.3	42.4	45.3	59.9	56.2	27.7
20	RMSprop	10	20.2	37.4	47.0	43.7	44.2	26.1
15	sgdm	20	3.8	23.1	17.5	15.9	14.1	19.8
20	sgdm	20	27.3	60.5	74.8	69.3	73.9	27.4
20	sgdm	20	23.8	51.0	63.6	66.8	56.5	26.7
15	Adam	20	3.7	11.6	7.5	7.4	9.5	71.7
20	Adam	20	6.1	13.3	28.7	18.5	40.8	32.2
20	Adam	20	5.6	17.9	27.4	22.5	39.3	94.0
15	RMSprop	20	3.8	11.7	14.5	19.2	11.7	17.9
20	RMSprop	20	6.1	42.2	54.7	47.5	42.6	22.3
20	RMSprop	20	19.1	30.3	44.7	51.7	37.1	26.9
15	sgdm	50	3.2	15.3	9.2	7.7	13.8	19.6
20	sgdm	50	18.2	32.2	60.3	42.8	30.2	28.9
20	sgdm	50	9.4	55.2	56.0	16.0	32.4	32.4
15	Adam	50	3.4	10.4	9.8	9.9	39.1	22.6
20	Adam	50	8.3	80.3	19.8	82.3	79.6	34.8
20	Adam	50	7.2	9.6	41.4	10.0	27.6	23.6
15	RMSprop	50	3.4	18.7	10.0	8.3	11.2	<u>17.5</u>
20	RMSprop	50	5.6	33.2	25.7	34.8	34.4	22.4
20	RMSprop	50	5.4	22.8	45.3	20.0	34.7	29.2
15	sgdm	100	3.9	10.6	7.9	7.7	<u>7.7</u>	21.4
20	sgdm	100	9.6	22.1	39.4	39.7	30.3	23.8
20	sgdm	100	13.7	17.1	52.8	26.3	37.1	30.5
15	Adam	100	2.7	16.6	80.3	7.2	18.2	21.9
20	Adam	100	<u>2.6</u>	38.9	79.9	80.1	31.1	25.7
20	Adam	100	3.4	80.0	79.7	80.9	80.3	28.6
15	RMSprop	100	4.8	11.2	<u>7.2</u>	8.1	9.5	18.1
20	RMSprop	100	7.1	66.0	46.0	28.6	30.9	24.0
20	RMSprop	100	5.6	29.5	26.9	18.5	29.3	22.9
Max			71.9	80.3	80.3	82.3	80.3	94.1
Mean			10.4	30.7	39.4	33.7	35.6	30.7
Min			2.6	8.9	7.2	7.1	7.7	17.5

Table 2. Comparative misclassification (%) results with co-occurrence [5], best filtering result from Randen [52], p_8 and LBP [53], Watershed [54], Multiresolution sub-band filtering (MSBF) [8] and U-Net [46]. (Bold is the best for each image).

Method	Figures						Average
	a	b	c	d	e	f	
Co-occurrence [5]	9.9	27.0	26.1	51.1	35.7	49.6	33.23
Best in Randen [59]	7.2	18.9	20.6	16.8	17.2	34.7	19.23
p_8 [60]	7.4	12.8	15.9	18.4	16.6	27.7	16.46
LBP [60]	6.0	18.0	12.1	9.7	11.4	17.0	12.36
Watershed [54]	7.1	10.7	12.4	11.6	14.9	20.0	12.78
MSBF [8]	2.8	14.8	8.4	7.3	4.3	17.9	9.25
U-Net [46]	2.6	8.9	7.2	7.1	7.7	17.5	8.50

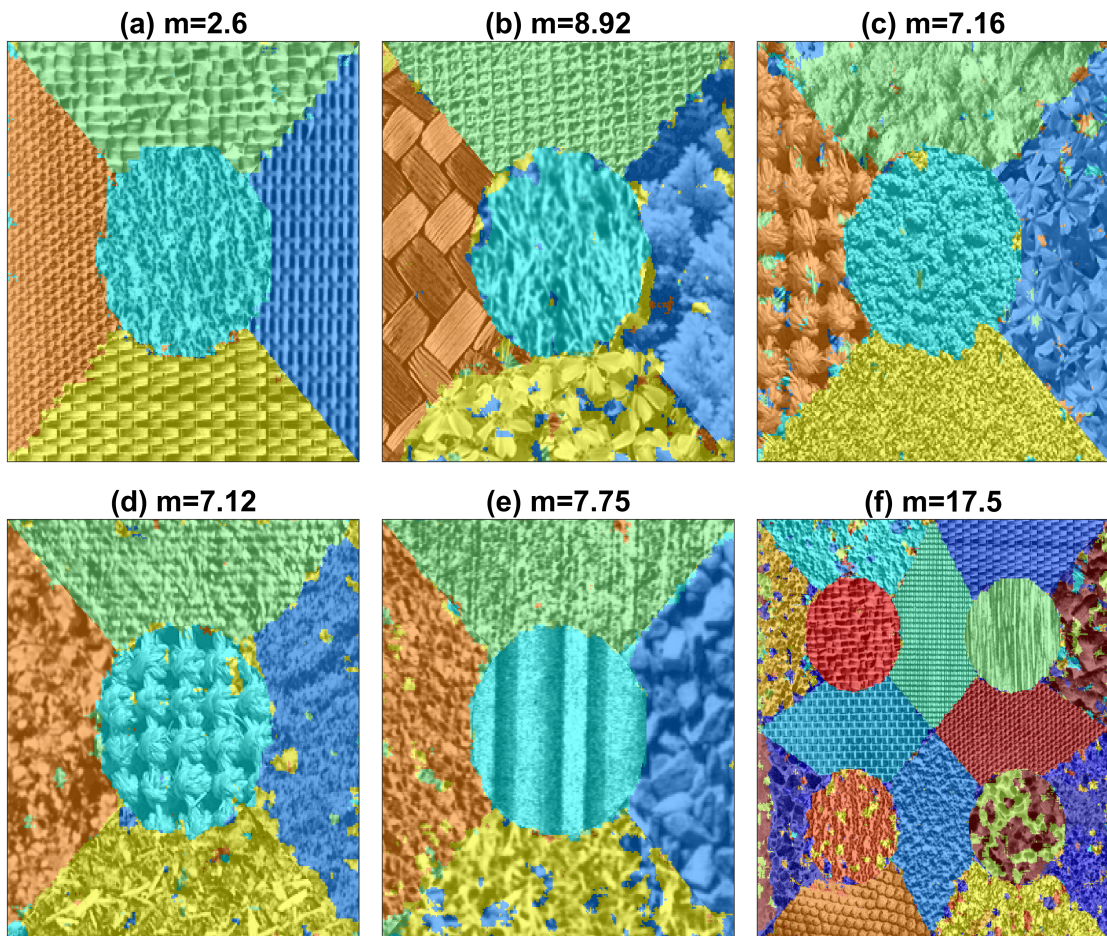


Figure 6. (a-f) Results of the segmentation with U-Nets for the six texture arrangements. The misclassification (%) is shown in each case. The classes are shown as overlaid colours.

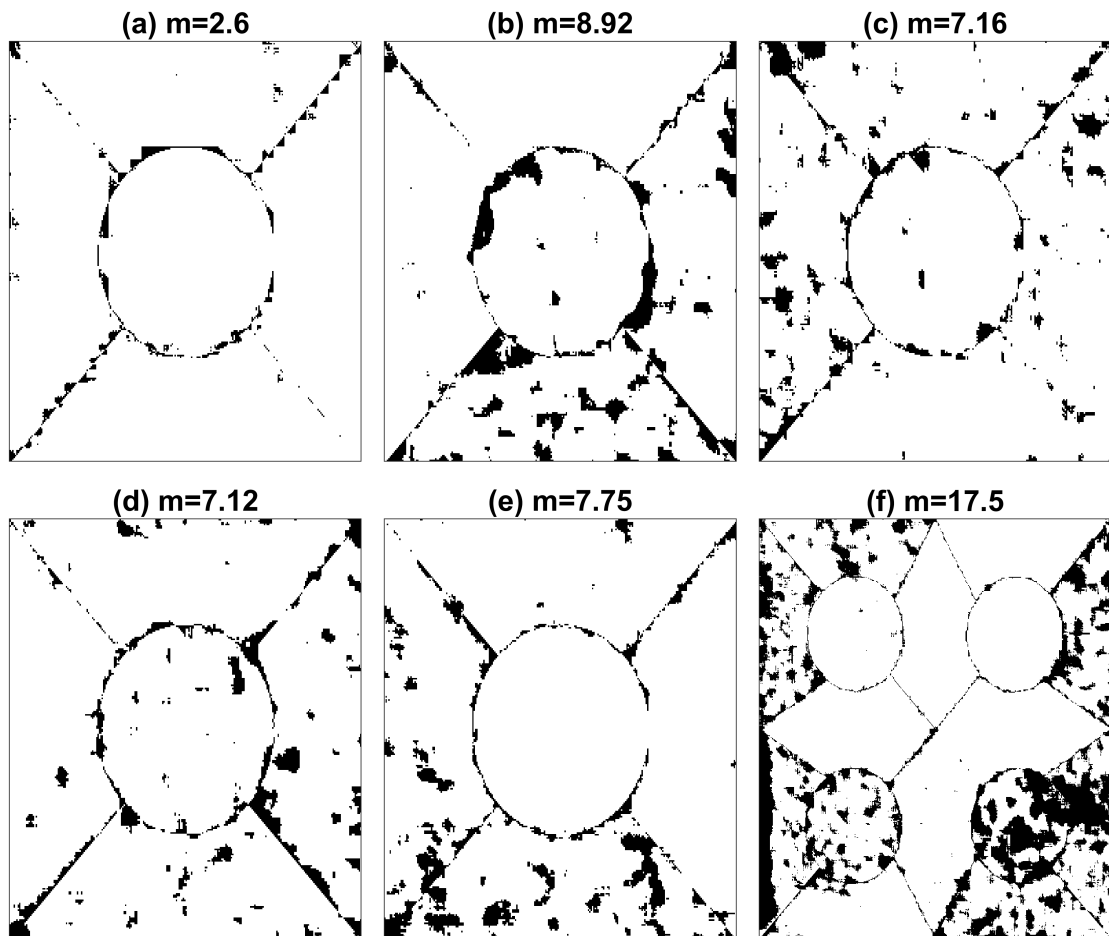


Figure 7. (a-f) Results of the segmentation with U-Nets for the six texture arrangements. The misclassification (%) is shown in each case. Pixels that are correctly classified appear in white.

110 4. Discussion

111 The results provided by the U-Net algorithm provided interesting results. First, overall, the
 112 segmentation results provided by the U-Net were better than all the traditional algorithms and were
 113 the best four of the six images. In some cases, the results were very close to the second best option
 114 (a,d,f) and in two cases (e,f) traditional algorithms provided better results. Second, there was a great
 115 variability in the results produced by the different configurations. It was surprising that the maximum
 116 value of the misclassification in some cases was extremely high, 80% in the cases of 5 textures and
 117 94% in the case of 16 textures, those cases are equivalent of selecting a single class for all textures.
 118 Third, three of the best results were obtained with 100 epochs, 2 with 10 epochs, and 1 with 50, which
 119 is counter-intuitive as it would be expected that longer training times would provide better results.
 120 Fourth, three of the best results were provided by RMSprop optimisation, two by Adam and one by
 121 sgdm. Finally, and perhaps the most surprising result was that the results provided by the two 20 layer
 122 configurations were very different. In a few cases the result were equal (e.g. image c, sgdm, 10 epochs;
 123 image b, Adam, 10 epochs) but in others the variation was huge (e.g. image b, Adam, 50 epochs).

124 In terms of texture, it can be highlighted that not all textures are the same, the five textures of
 125 image (a) are far easier to distinguish and correctly segment than those of image (b) and image (f). The
 126 U-Net was capable of segmenting these textures with accuracy comparable or better than traditional
 127 techniques. There are many other configuration parameters that could be varied; *learning rate, batch size,*
 128 *variations of the training data, different number of layers*, but for the purpose of this work, the results show
 129 first, the capability of deep learning architectures for segmentation of textured images and second, in
 130 some cases better results than traditional methodologies. However, the configuration of the network

is not trivial and variations of some parameters can provide sub-optimal results. The experiments conducted in this work did not provide conclusive evidence for the selection of any of the parameters evaluated. Furthermore, training of the networks requires considerable resources. The training times for the images with 5 textures took around 5 hours and for the image with 16 textures around 96 hours on a Mac Pro (Late 2013) with a 3.7GHz Quad-Core and 32 GB Memory with Dual AMD FirePro D300 graphics processors.

Therefore, it can be concluded that U-Net convolutional neural networks can be used for texture segmentation and provide results that are comparable or better than traditional texture algorithms. Furthermore, these results encourage the application of deep learning to other areas, like the texture of voice spectrograms [61]. We can even hypothesise that the images in two dimensions can be decomposed into one-dimensional signals and revisit the analysis of voice signals for the segmentation and classification of phonemes as it was done with early versions of Convolutional Neural Networks [62].

144

145 **Acknowledgments:** This work was funded by the Leverhulme Trust, Research Project Grant RPG-2017-054.

146 References

1. Bigun, J. Multidimensional Orientation Estimation with Applications to Texture Analysis and Optical Flow. *IEEE Transactions on Pattern Analysis and Machine Intelligence* **1991**, *13*, 775–790.
2. Bovik, A.C.; Clark, M.; Geisler, W.S. Multichannel Texture Analysis Using Localized Spatial Filters. *IEEE Transactions on Pattern Analysis and Machine Intelligence* **1990**, *12*, 55–73.
3. Cross, G.R.; Jain, A.K. Markov Random Field Texture Models. *IEEE Transactions on Pattern Analysis and Machine Intelligence* **1983**, *5*, 25–39.
4. Haralick, R.M. Statistical and Structural Approaches to Texture. *Proceedings of the IEEE* **1979**, *67*, 786–804.
5. Haralick, R.M.; Shanmugam, K.; Dinstein, I. Textural Features for Image Classification. *IEEE Transactions on Systems, Man and Cybernetics* **1973**, *3*, 610–621.
6. Tamura, H.; Mori, S.; Yamawaki, T. Texture Features corresponding to Visual Perception. *IEEE Transactions on Systems, Man and Cybernetics* **1978**, *8*, 460–473.
7. Tuceryan, M.; Jain, A.K. Texture Analysis. *Handbook of Pattern Recognition and Computer Vision*, Second ed.; Chen, C.H.; Pau, L.F.; Wang, P.S.P., Eds. World Scientific Publishing, 1998, pp. 207–248.
8. Reyes-Aldasoro, C.C.; Bhalerao, A. The Bhattacharyya Space for Feature Selection and Its Application to Texture Segmentation. *Pattern Recogn.* **2006**, *39*, 812–826. doi:10.1016/j.patcog.2005.12.003.
9. Bouman, C.; Liu, B. Multiple Resolution Segmentation of Textured Images. *IEEE Transactions on Pattern Analysis and Machine Intelligence* **1991**, *13*, 99–113.
10. Jain, A.K.; Farrokhnia, F. Unsupervised texture segmentation using Gabor filters. *Pattern Recognition* **1991**, *24*, 1167–1186.
11. Kadyrov, A.; Talepboun, A.; Petrou, M. Texture Classification with Thousand of Features. British Machine Vision Conference (BMVC); , 2002; pp. 656–665.
12. Kervrann, C.; Heitz, F. A Markov Random Field model-based approach to unsupervised texture segmentation using local and global spatial statistics. *IEEE Transactions on Image Processing* **1995**, *4*, 856–862.
13. Unser, M. Texture Classification and Segmentation Using Wavelet Frames. *IEEE Transactions on Image Processing* **1995**, *4*, 1549–1560.
14. Weszka, J.; Dyer, C.; Rosenfeld, A. A comparative Study of Texture Measures for Terrain Classification. *IEEE Transactions Systems, Man and Cybernetics* **1976**, *6*, 269–285.
15. Tai, C.; Baba-Kishi, K. Microtexture studies of PST and PZT Ceramics and PZT Thin Film by Electron Backscatter Diffraction Patterns. *Textures and Microstructures* **2002**, *35*, 71–86.
16. Carrillat, A.; Randen, T.; Snneland, L.; Elvebakk, G. Seismic stratigraphic mapping of carbonate mounds using 3D texture attributes. Extended Abstracts, Annual Meeting, European Association of Geoscientists and Engineers; , 2002.
17. Randen, T.; Monsen, E.; Abrahamsen, A.; Hansen, J.O.; Schlaf, J.; Snneland, L. Three-dimensional texture attributes for seismic data analysis. *Ann. Int. Mtg., Soc. Expl. Geophys., Exp. Abstr.*; , 2000.

181 18. Thybo, A.K.; Martens, M. Analysis of sensory assessors in texture profiling of potatoes by multivariate
182 modelling. *Food Quality and Preference* **2000**, *11*, 283–288. doi:10.1016/S0950-3293(99)00045-2.

183 19. Létal, J.; Jirák, D.; Šuderlová, L.; Hájek, M. MRI ‘texture’ analysis of MR images of apples during ripening
184 and storage. *LWT - Food Science and Technology* **2003**, *36*, 719–727. doi:10.1016/S0023-6438(03)00099-9.

185 20. Lizarraga-Morales, R.A.; Sanchez-Yanez, R.E.; Baeza-Serrato, R. Defect detection on patterned fabrics using
186 texture periodicity and the coordinated clusters representation. *Textile Research Journal* **2017**, *87*, 1869–1882,
187 [<https://doi.org/10.1177/0040517516660885>]. doi:10.1177/0040517516660885.

188 21. Bianconi, F.; González, E.; Fernández, A.; Saetta, S.A. Automatic classification of granite tiles through colour
189 and texture features. *Expert Systems with Applications* **2012**, *39*, 11212–11218. doi:10.1016/j.eswa.2012.03.052.

190 22. Kovalev, V.A.; Petrou, M.; Bondar, Y.S. Texture Anisotropy in 3D Images. *IEEE Transactions on Image
191 Processing* **1999**, *8*, 346–360.

192 23. Reyes-Aldasoro, C.C.; Bhalerao, A. Volumetric Texture Description and Discriminant Feature Selection for
193 MRI. Proceedings of Information Processing in Medical Imaging; Taylor, C.; Noble, A., Eds.; , 2003; pp.
194 282–293.

195 24. Lerski, R.; Straughan, K.; Schad, L.R.; Boyce, D.; Bluml, S.; Zuna, I. MR Image Texture Analysis - An
196 Approach to tissue Characterization. *Magnetic Resonance Imaging* **1993**, *11*, 873–887.

197 25. Schad, L.R.; Bluml, S.; Zuna, I. MR Tissue Characterization of Intracranial Tumors by means of Texture
198 Analysis. *Magnetic Resonance Imaging* **1993**, *11*, 889–896.

199 26. Reyes Aldasoro, C.C.; Bhalerao, A. Volumetric Texture Segmentation by Discriminant Feature
200 Selection and Multiresolution Classification. *IEEE Transactions on Medical Imaging* **2007**, *26*, 1–14.
201 doi:10.1109/TMI.2006.884637.

202 27. Zhan, Y.; Shen, D. Automated Segmentation of 3D US Prostate Images Using Statistical Texture-Based
203 Matching Method. Medical Image Computing and Computer-Assisted Intervention (MICCAI); , 2003; pp.
204 688–696.

205 28. Xie, J.; Jiang, Y.; tat Tsui, H. Segmentation of kidney from ultrasound images based on texture and shape
206 priors. *IEEE Transactions on Medical Imaging* **2005**, *24*, 45–57. doi:10.1109/TMI.2004.837792.

207 29. Hoffman, E.A.; Reinhardt, J.M.; Sonka, M.; Simon, B.A.; Guo, J.; Saba, O.; Chon, D.; Samra, S.; Shikata,
208 H.; Tschirren, J.; Palagyi, K.; Beck, K.C.; McLennan, G. Characterization of the Interstitial Lung Diseases
209 via Density-Based and Texture-Based Analysis of Computed Tomography Images of Lung Structure and
210 Function. *Academic Radiology* **2003**, *10*, 1104–1118.

211 30. Segovia-Martínez, M.; Petrou, M.; Kovalev, V.A.; Perner, P. Quantifying Level of Brain Atrophy Using
212 Texture Anisotropy in CT Data. Medical Imaging Understanding and Analysis; , 1999; pp. 173–176.

213 31. Ganeshan, B.; Goh, V.; Mandeville, H.C.; Ng, Q.S.; Hoskin, P.J.; Miles, K.A. Non-Small Cell
214 Lung Cancer: Histopathologic Correlates for Texture Parameters at CT. *Radiology* **2013**, *266*, 326–336.
215 doi:10.1148/radiol.12112428.

216 32. Sabino, D.M.U.; da Fontoura Costa, L.; Gil Rizzato, E.; Antonio Zago, M. A texture approach to leukocyte
217 recognition. *Real-Time Imaging* **2004**, *10*, 205–216. doi:10.1016/j.rti.2004.02.007.

218 33. Wang, X.; He, W.; Metaxas, D.; Mathew, R.; White, E. Cell Segmentation and Tracking using
219 Texture-Adaptive Snakes. 2007 4th IEEE International Symposium on Biomedical Imaging: From Nano to
220 Macro, 2007, p. 101–104. doi:10.1109/ISBI.2007.356798.

221 34. Kather, J.N.; Weis, C.A.; Bianconi, F.; Melchers, S.M.; Schad, L.R.; Gaiser, T.; Marx, A.; Zollner, F. Multi-class
222 texture analysis in colorectal cancer histology | Scientific Reports. *Scientific Reports* **2016**, *6*, 27988.

223 35. Dunn, D.; Higgins, W.; Wakeley, J. Texture segmentation using 2-D Gabor elementary functions. *IEEE
224 Transactions on Pattern Analysis and Machine Intelligence* **1994**, *16*, 130–149.

225 36. Bigun, J.; du Buf, J.M.H. N-Folded Symmetries by Complex Moments in Gabor Space and Their Application
226 to Unsupervised Texture Segmentation. *IEEE Transaction on Pattern Analysis and Machine Intelligence* **1994**,
227 *16*, 80–87.

228 37. Bianconi, F.; Fernández, A. Evaluation of the effects of Gabor filter parameters on texture classification.
229 *Pattern Recognition* **2007**, *40*, 3325 – 3335. doi:<https://doi.org/10.1016/j.patcog.2007.04.023>.

230 38. Rajpoot, N.M. Texture Classification Using Discriminant Wavelet Packet Subbands. Proceedings 45th IEEE
231 Midwest Symposium on Circuits and Systems (MWSCAS 2002); , 2002.

232 39. Chang, T.; Kuo, C.C.J. Texture Analysis and Classification with Tree-Structured Wavelet Transform. *IEEE
233 Transactions on Image Processing* **1993**, *2*, 429–441.

234 40. Chellappa, R.; Jain, A. *Markov Random Fields*; Academic Press: Boston, 1993.

235 41. Krizhevsky, A.; Sutskever, I.; Hinton, G.E. ImageNet Classification with Deep Convolutional Neural Networks. Proceedings of the 25th International Conference on Neural Information Processing Systems - Volume 1. Curran Associates Inc., 2012, NIPS'12, p. 1097–1105. event-place: Lake Tahoe, Nevada.

236 42. Zeiler, M.D.; Fergus, R. Visualizing and Understanding Convolutional Networks. Computer Vision – ECCV 2014; Fleet, D.; Pajdla, T.; Schiele, B.; Tuytelaars, T., Eds. Springer International Publishing, 2014, Lecture Notes in Computer Science, p. 818–833.

237 43. Simonyan, K.; Zisserman, A. Very Deep Convolutional Networks for Large-Scale Image Recognition. *arXiv:1409.1556 [cs]* **2014**. arXiv: 1409.1556.

238 44. Russakovsky, O.; Deng, J.; Su, H.; Krause, J.; Satheesh, S.; Ma, S.; Huang, Z.; Karpathy, A.; Khosla, A.; Bernstein, M.; Berg, A.C.; Fei-Fei, L. ImageNet Large Scale Visual Recognition Challenge. *International Journal of Computer Vision (IJCV)* **2015**, *115*, 211–252. doi:10.1007/s11263-015-0816-y.

239 45. Andrarczyk, V.; Whelan, P.F., Chapter 4 - Deep Learning in Texture Analysis and Its Application to Tissue Image Classification. In *Biomedical Texture Analysis*; Depeursinge, A.; S. Al-Kadi, O.; Mitchell, J.R., Eds.; Academic Press, 2017; p. 95–129. doi:10.1016/B978-0-12-812133-7.00004-1.

240 46. Ronneberger, O.; Fischer, P.; Brox, T. U-Net: Convolutional Networks for Biomedical Image Segmentation. Medical Image Computing and Computer-Assisted Intervention – MICCAI 2015; Navab, N.; Hornegger, J.; Wells, W.M.; Frangi, A.F., Eds. Springer International Publishing, 2015, Lecture Notes in Computer Science, p. 234–241.

241 47. Zhang, Z.; Liu, Q.; Wang, Y. Road Extraction by Deep Residual U-Net. *IEEE Geoscience and Remote Sensing Letters* **2018**, *15*, 749–753. doi:10.1109/LGRS.2018.2802944.

242 48. Jansson, A.; Humphrey, E.J.; Montecchio, N.; Bittner, R.M.; Kumar, A.; Weyde, T. Singing Voice Separation with Deep U-Net Convolutional Networks. ISMIR, 2017.

243 49. Dong, H.; Yang, G.; Liu, F.; Mo, Y.; Guo, Y. Automatic Brain Tumor Detection and Segmentation Using U-Net Based Fully Convolutional Networks. Medical Image Understanding and Analysis; Valdés Hernández, M.; González-Castro, V., Eds. Springer International Publishing, 2017, Communications in Computer and Information Science, p. 506–517.

244 50. Falk, T.; Mai, D.; Bensch, R.; Çiçek, Ö.; Abdulkadir, A.; Marrakchi, Y.; Böhm, A.; Deubner, J.; Jäckel, Z.; Seiwald, K.; et al.. U-Net: deep learning for cell counting, detection, and morphometry. *Nature Methods* **2019**, *16*, 67. doi:10.1038/s41592-018-0261-2.

245 51. Brodatz, P. *Textures: A photographic album for artists and designers*; Dover: New York, U.S.A, 1996.

246 52. Randen, T.; Husøy, J.H. Filtering for Texture Classification: A Comparative Study. *IEEE Transactions on Pattern Analysis and Machine Intelligence* **1999**, *21*, 291–310.

247 53. Ojala, T.; Valkealahti, K.; Oja, E.; Pietikäinen, M. Texture discrimination with multidimensional distributions of signed gray level differences. *Pattern Recognition* **2001**, *34*, 727–739.

248 54. Malpica, N.; Ortúñoz, J.E.; Santos, A. A multichannel watershed-based algorithm for supervised texture segmentation. *Pattern Recognition Letters* **2003**, *24*, 1545–1554.

249 55. Petrou, M.; Garcia-Sevilla, P. *Image Processing: Dealing with Texture*; John Wiley & Sons, 2006.

250 56. Reyes-Aldasoro, C.C.; Bhale Rao, A.H. Volumetric Texture Analysis in Biomedical Imaging. *Biomedical Diagnostics and Clinical Technologies: Applying High-Performance Cluster and Grid Computing*; Pereira, M.; Freire, M., Eds. IGI Global, 2011, p. 200–248.

251 57. Mirmehdi, M.; Xie, X.; Suri, J. *Handbook of Texture Analysis*; Imperial College Press, 2009.

252 58. Kingma, D.P.; Ba, J. Adam: A Method for Stochastic Optimization. <http://arxiv.org/abs/1412.6980> **2014**.

253 59. Randen, T.; Husøy, J.H. Texture segmentation using filters with optimized energy separation. *IEEE Transactions Image Processing* **1999**, *8*, 571–582.

254 60. Ojala, T.; Pietikäinen, M.; Harwood, D. A Comparative Study of Texture Measures with Classification based on Feature Distributions. *Pattern Recognition* **1996**, *29*, 51–59.

255 61. Verhoeven, J.; Miller, N.R.; Daems, L.; Reyes-Aldasoro, C.C. Visualisation and Analysis of Speech Production with Electropalatography. *Journal of Imaging* **2019**, *5*, 40. doi:10.3390/jimaging5030040.

256 62. Waibel, A.; Hanazawa, T.; Hinton, G.; Shikano, K.; Lang, K.J. Phoneme recognition using time-delay neural networks. *IEEE Transactions on Acoustics, Speech, and Signal Processing* **1989**, *37*, 328–339. doi:10.1109/29.21701.